Volume 1 | Number 1 | Jan 2013 | Pages 1–100

Chemical Science

www.rsc.org/chemicalscience

ROYAL SOCIETY OF CHEMISTRY

ROYAL SOCIETY OF CHEMISTRY

www.rsc.org/chemicalscience

Chemical Science

EDGE ARTICLE

A dual-responsive nanocapsule *via* disulfide-induced self-assembly for therapeutic agent delivery

Wenhai Lin,[ab] Tingting Sun,[ab] Zhigang Xie,[a]* Jingkai Gu[c] and Xiabin Jing[a]

One-step synthesis of fluorescent molecules (SNBDP) containing one disulfide bond and two *o*-nitro benzyl groups was demonstrated *via* multi-component Passerini reaction. This hydrophobic SNBDP could self-assemble into nanocapsules (SNBDP NCs) in aqueous solution *via* disulfide-induced assembly. The obtained nanocapsules were stable in aqueous solution for several weeks and exhibited enhanced fluorescence when nanocapsules were destroyed due to disaggregation-induced emission. The nanocapsules not only were reduction-sensitive and light-responsive, but also could be endocytosed by HeLa cells for cellular imaging. The enhanced fluorescence in the glutathione (GSH) pretreated HeLa cells showed that the compound was reduction-sensitive in living cells. *In vitro* WST-8 assays showed the nanocapsules were biocompatible and could further be used as drug delivery carriers. Indocyanine green (ICG), a NIR dye for clinic approved, was loaded into the nanocapsules (ICG@SNBDP NCs). ICG@SNBDP NCs showed the enhanced photothermal efficacy compared with same concentration of free ICG under 808 nm laser irradiation. Consequently, ICG@SNBDP NCs upon NIR irradiation can effectively kill cancer cells through local hyperthermia. These results highlight the potential of disulfide-induced nanocapsules as smart nanoparticles for celluar imaging and therapeutic agent delivery.

Introduction

Self-assembly of small molecules (SASM) is a fascinating and useful method to fabricate various functional nanomaterials. Compared with macromolecular counterparts, SASM has shown great advantages because of precise molecular structure and repeatable large-scale synthesis.[1, 2] Programmed SASM could be achieved by using different supramolecular chemistry, such as hydrophobic interactions, electrostatic interactions, π-π interactions and hydrogen-bond interactions.[3, 4] However, development of SASM is relatively slow compared to the self-assembly of polymers.[5-7] Up to now, SASM is mainly realized by choosing the amphiphilic small molecules or π-conjugated monomers.[8-10] For example, Yan et al. have reported the nanodrug from assembly of amphiphilic drug-drug conjugate for cancer therapy.[11] Our previous work has demonstrated that unadulterated BODIPY (4, 4-difluoro-4-bora-3a,4a-diaza-s-indacene) dimer could self-assemble into fluorescent

nanoparticles for cellular imaging because of its π-conjugated structure.[12] Unfortunately, most of the drugs and dyes are hydrophobic and not easy to be modified by hydrophilic molecules, and cannot self-assemble into nanoparticles. It is desired to develop some new ways to make functional nanomaterials. Very recently, nanomedicines made *via* disulfide bond bridge have been demonstrated and caught our great attention.[13] Disulfide-induced nanomedicines (DSINMs) have been promoted and stabilized by the insertion of a single disulfide bond into hydrophobic molecules, in order to balance the competition between intermolecular forces. But it is not clear whether this disulfide-induced assembly is universal for other hydrophobic molecules. It is well-known that hydrophobic small molecules without π-conjugated structures can't self-assemble into stable nanoparticles. Up to now, no work on disulfide-induced fluorescent nanoparticles was reported.

Compared to traditional fluorescent organic dyes, fluorescent nanoparticles show unique chemical and optical properties, such as brighter fluorescence, higher photostability and better biocompatibility, for their application in bioimaging and diagnostic.[14-17] Moreover, fluorescent nanoparticles could provide a versatile platform for loading drugs or bioactive molecules. These properties make them useful in medical and biological fields.[18-20] The ideal fluorescent nanoparticles should possess super brightness, excellent photostability and good biocompatibility.[21, 22]

BODIPY (BDP) dyes have drawn much attention due to their excellent photophysical properties and been widely used in cellular imaging and chemical sensor.[23, 24] It has been reported that fluorescent BDP could be adapted to multi-component reaction chemistry with high fluorescence quantum yields and good cell

a.† State Key Laboratory of Polymer Chemistry and Physics, Changchun Institute of Applied Chemistry, Chinese Academy of Sciences, 5625 Renmin Street, Changchun, Jilin 130022, P. R. China. E-mail: xiez@ciac.ac.cn; Fax/Tel: +86 431 85262775
b. University of Chinese Academy of Sciences, Beijing 100049, P. R. China
c. Research Center for Drug Metabolism, College of Life Sciences, Jilin University, Changchun 130012, P. R. China
† Electronic Supplementary Information (ESI) available: Experimental section, MALDI-TOF-MS spectra of the SNBDP, the changes of the diameter and PdI in PBS with FBS FT-IR of SNBDP NCs before and after light irradiation, illustration of the formation of supramolecular vesicles, cell viability of HeLa cells incubated with SNBDP NCs, representative CLSM images of HeLa cells for 0.5 h without pretreatment and pretreated with 10 mM GSH, the size of RhB@SNBDP NCs measured by DLS, TEM images and fluorescence spectra of RhB@SNBDP NCs and RhB in water, TEM images of the ICG@SNBDP NCs, representative CLSM images of HeLa cells incubated with ICG@SNBDP NCs for 0.5 h and 2 h and cell viability after water-bath hyperthermia. See DOI: 10.1039/x0xx00000x
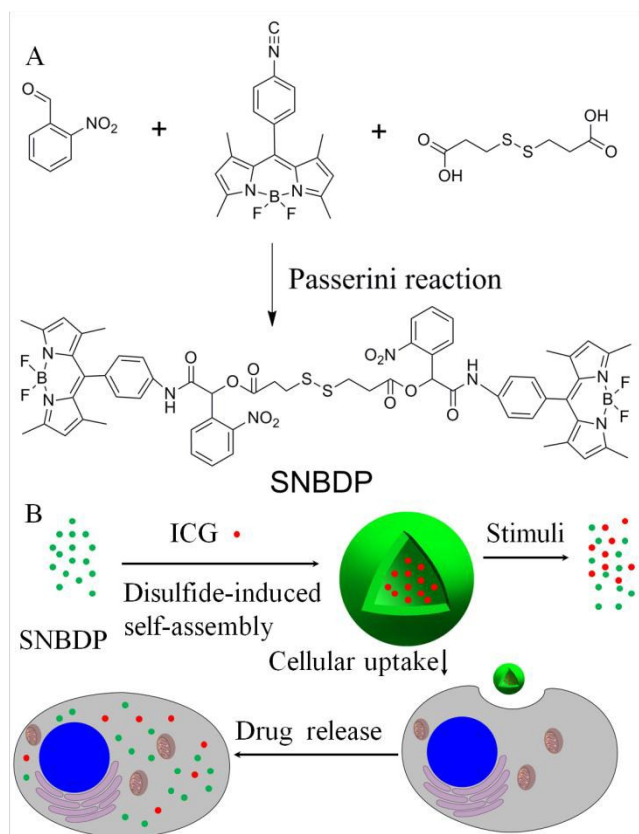
Scheme 1. (A) Synthesis of the SNBDP *via* multi-component Passerini reaction. (B) A schematic illustration of the self-assembly,disassembly and celluar uptake of SNBDP NCs.

permeability for *in vivo* imaging of phagocytic macrophages.[25] However, the BDP derivatives couldn't directly self-assemble into nanostructures in aqueous solution. It is still a great challenge to prepare fluorescent nanoparticles from versatile BDP dyes.

In this report, a dual-responsive fluorescent molecule (SNBDP, Scheme 1A) was synthesized by way of one-pot multi-component Passerini reaction from 4,4-Difluoro-8-(4-isocyanophenyl)-3,5-dimethyl-4-bora-3a,4a-diaza-indacene (NC-BDP), 3,3-dithiodipropionic acid and *o*-nitrobenzaldehyde. SNBDP could self-
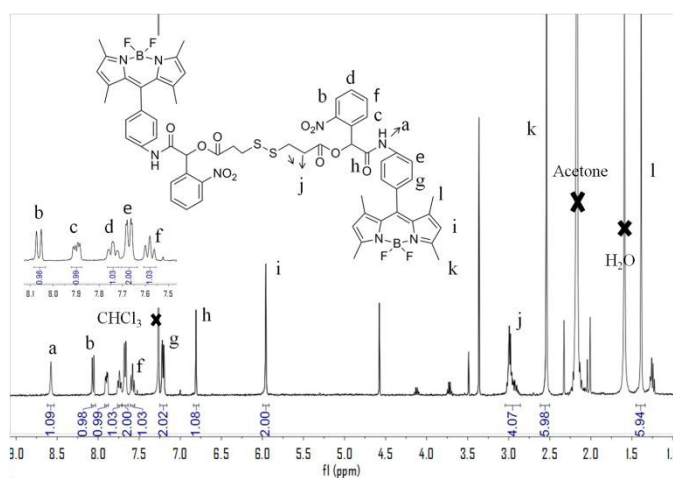

Fig. 1 ^{1}H NMR characterization of the SNBDP.

assemble into nanocapsules (SNBDP NCs) by virtue of the disulfide bond bridge. The self-assembly and stimuli-induced disassembly behaviours of SNBDP NCs were investigated in detail. Furthermore, SNBDP NCs could be internalized and disassembled to emit green fluorescence for bioimaging. ICG were loaded into the NCs to exhibit the potential applications for drug delivery (Scheme 1B).

Results and discussion

Synthesis and characterization of the NCs

Three-component Passerini reaction could combine isocyanides, aldehydes, and carboxylic acids into the ester and amide linkages *via* an atom-economic way. This reaction has been employed to synthesize diverse monomers and functional polymers due to the mild conditions without catalysts and tolerance to many functional groups.[26-29] We have reported that reduction-sensitive amphiphilic copolymers for drug delivery[30] and cross-linked polymers for photocatalysis *via* Passerini reaction.[31] In this work, multi-component Passerini reaction was used to synthesize the target dye molecules.

Firstly, 4,4-Difluoro-8-(4-isocyanophenyl)-3,5-dimethyl -4-bora- 3a,4a-diaza-indacene (NC-BDP) was synthesized according to the literature methods.[25] Then NC-BDP, 3,3-dithiodipropionic acid and *o*-nitrobenzaldehyde were mixed in dichloromethane and stirred at room temperature for 4 days (Scheme 1A). After purification on a silica gel column, the SNBDP was obtained and characterized by proton nuclear magnetic resonance (^{1}H NMR) and matrix-assisted laser desorption/ionization time-of-flight mass spectrometry (MALDI-TOF MS). As shown in Fig. 1, all the protons corresponding to the compound could be clearly resolved in
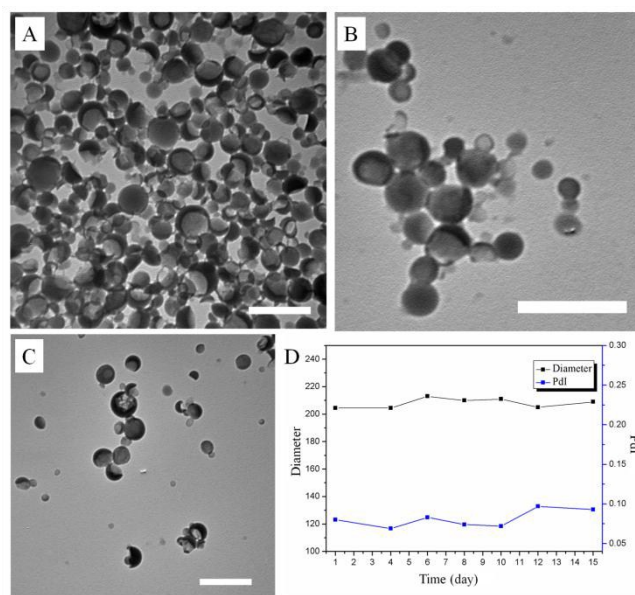
Fig. 2 (A) and (B) TEM images of SNBDP NCs. (C) TEM images of SNBDP NCs after stored for a month . (D) The changes of the diameter and PdI with different times measured by DLS. Scale bar, 500 nm.

the ^{1}H NMR spectrum, and the integration ratios of these peaks agreed well with that of theoretical calculation. More importantly, the signals at 8.57 ppm and 6.76 ppm for proton of imine and methine indicated that NC-BDP was successfully incorporated into SNBDP through Passerini reaction. The peak at 1210.4 in the MALDI-TOF MS spectrum is close to the theoretical molecular weight of SNBDP (Fig. S1†), further confirming the successful synthesis of SNBDP.

Interestingly, SNBDP could self-assemble into nanocapsules (SNBDP NCs) in aqueous solution *via* simple nano-precipitation method. Briefly, the tetrahydrofuran (THF) solution of SNBDP was added into water under stirring and then dialyzed to remove THF. The morphology and size distribution of SNBDP NCs were characterized by transmission electron microscopy (TEM) and dynamic light scattering (DLS), respectively. The TEM image in Fig. 2A showed a typical vesicular structure with an average diameter of about 200 nm. The partially collapsed morphologies further confirmed their vesicular structure in Fig. 2B. The morphologies of SNBDP NCs were kept even after storing for one month (Fig. 2C). Moreover, the diameter and the polydispersity index (PdI) measured by DLS almost kept unchanged in half a month (Fig. 2D). These results demonstra-
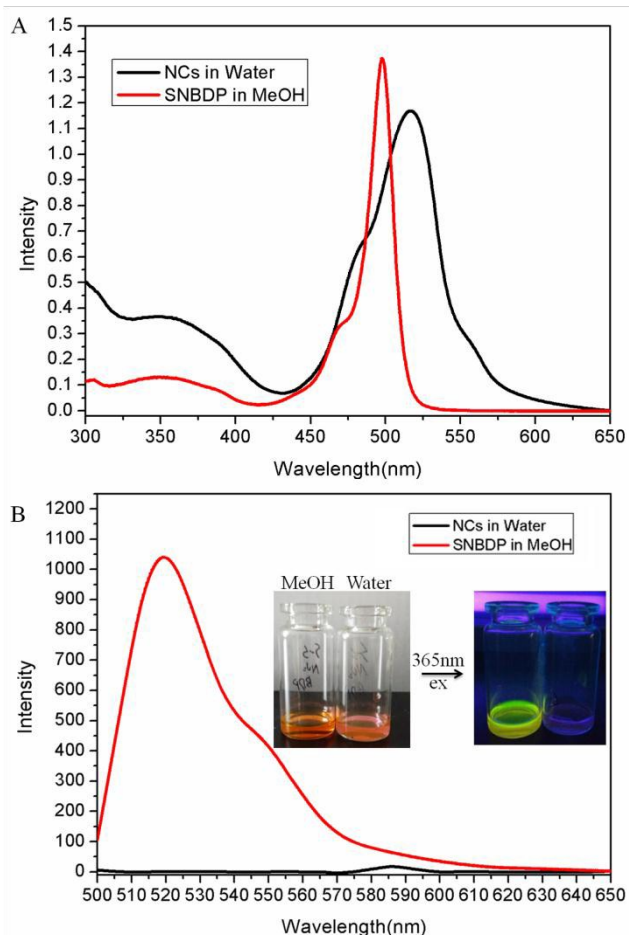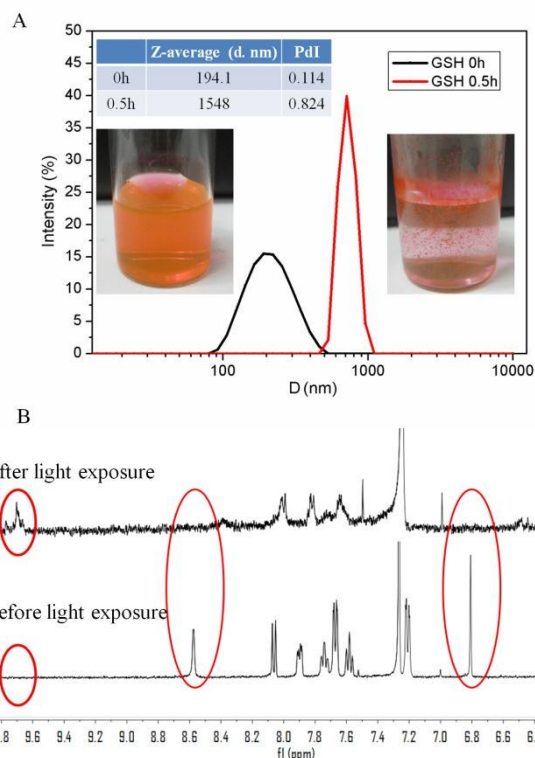
Fig. 4 (A) Reduction-induced disassembly resulting in size changes of SNBDP NCs. (B) The magnetic resonance spectra after and before light exposure.

ted that SNBDP NCs were stable in aqueous solution. As shown in Fig. 2D, the average diameter of SNBDP NCs measured by DLS was 204 nm, which was consistent with that observed by TEM. SNBDP NCs also exhibited favorable structural stability in physiological environment as evidenced by the unaltered particle size and PdI observed by incubating the NCs in PBS (pH 7.4) containing FBS (10%) at 37 $^{\circ}$C for up to 24 h (Fig. S2†).

The optical properties of the SNBDP NCs and SNBDP were studied by UV-vis absorption and photoluminescence spectra. As shown in Figure 3, although both of them exhibited similar absorption spectrum, the maximum absorption band of SNBDP NCs in water was centred at 516 nm, which was red-shifted by 20 nm relative to that of SNBDP in MeOH (Fig. 3A). Bathochromic shift absorption band of NCs indicated a J-aggregate of SNBDP in aqueous solution, which is consistent to the reported the aggregation of BODIPY.[32, 33] The maximum fluorescence wavelength was seen at 520 nm for SNBDP, but almost no fluorescence was observed for SNBDP NCs due to aggregation-caused quenching (ACQ) (Fig. 3B). To visually observe the phenomenon of ACQ,[34] the photos of SNBDP NCs and SNBDP were taken under the 365 nm light irradiation. As shown in Figure 3B, SNBDP in MeOH emitted a strong yellow-green fluorescence while no fluorescence was observed for SNBDP NCs.

For the vesicular aggregates, the possible mechanism was present based on the results of calculated electron density distribution. The optimized ground-state geometrical structure was optimized using density functional theory (DFT) at B3LYP/6-31G* level.[35-37] The calculated electron density distribution was interesting. BDP fragments on the ends of the

Fig. 3 (A) UV-vis absorption and (B) fluorescence spectra of SNBDP NCs in water and the SNBDP in MeOH.
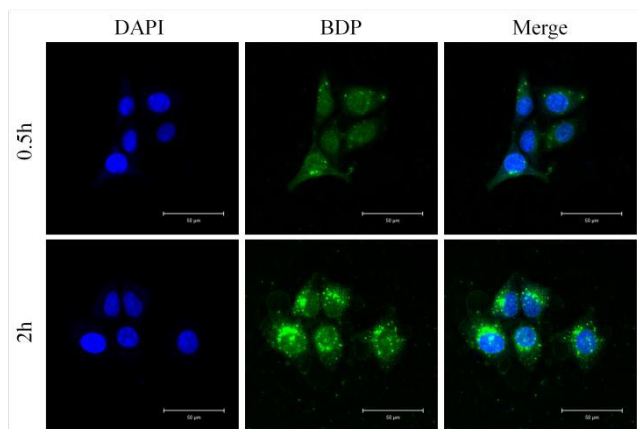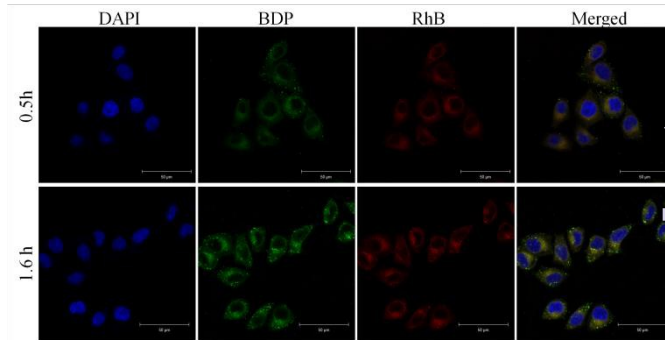
Fig. 5 Representative CLSM images of HeLa cells incubated with SNBDP NCs for 0.5 h and 2 h. For each panel, the images from left to right show cell nuclei stained by DAPI (blue), BDP fluorescence in cells (green), and overlays of both images. Scale bar, 50 μm.

molecule carried positive charge (+0.60) and the central S-S fragments carried negative charge (-0.60). So we predicted that the major reason of the formation of the nanoparticles was electrostatic forces as shown in Fig. S3A. As shown in Fig. S3B, the J-type arrangement of SNBDP units firstly formed single layers through the electrostatic interactions, then the vesicles was obtained *via* hydrophobic and π-π interactions between different layer of SNBDP. Some similar vesicular aggregates have been reported by using BODIPY molecules.[38,39] Transitioning from small molecular to supramolecular capsules also can be seen in recent review.[40] It is not surprise to obtain the nanocapsule in this work.

Dual-responsive behaviours of NCs

The reduction-induced dissociation of disulfide bonds in SNBDP NCs was monitored by DLS in the presence of 10 mM GSH (Fig. 4A). The increase in the diameter of SNBDP NCs from 194.1 nm to 1548 nm was observed after half an hour. The PDI also increased from 0.114 to 0.824, which confirmed the disassembly of SNBDP NCs. The solution changed from clear to muddy, and a large number of precipitates were found (Fig. 4A, right photo). The formation of precipitates were attributed to the disassembly of SNBDP NCs, resulting in rearrangement of hydrophobic fragments into large agglomerates.[41] These results demonstrate SNBDP NCs are reduction-sensitive and could be destroyed in the presence of reducing agents.

Owing to their non-invasiveness and the possibility of remote spatiotemporal control, a large variety of photoresponsive systems has been engineered in the past few years.[42, 43] *O*-nitro benzyl and its derivatives have been widely used as photocleavable groups in drug release.[44] Upon exposure to 365 nm light, effective photolysis of SNBDP NCs was evidenced by ^{1}H NMR (Fig. 4B) and Fourier transform infrared (FT-IR) spectroscopy (Fig. S4†). The characteristic signals at 8.57 ppm and 6.76 ppm disappeared upon exposure light irradiation (Fig. 4B). Moreover, the appearance of signal at 9.73 ppm indicated the SNBDP was cleaved into carbonyl photoproducts. The photolysis was further corroborated by FT-IR spectroscopy where peaks at 3400 cm^{-1} (broad) and 1740 cm^{-1} appeared in the spectrum of the irradiated sample,

Fig. 6 Representative CLSM images of HeLa cells incubated with RhB@SNBDP NCs for 0.5 h and 1.6 h. For each panel, the images from left to right show cell nuclei stained by DAPI (blue), BDP fluorescence (green), RhB fluorescence (red) and overlays of both images. Scale bar, 50 μm.

indicating of the formation of photoproducts containing hydroxyl and carbonyl (Fig. S4†).

Intracellular uptake and bioimaging of SNBDP NCs

The biocompatibility of nanomaterials is very important for their biomedical applications. The *in vitro* cytotoxicities of SNBDP NCs toward human cervical carcinoma (HeLa) cells were evaluated by cell counting kit-8 (CCK-8).[45, 46] Fig. S5 showed the viability of cells incubated with various concentrations of SNBDP NCs for 24 h. SNBDP NCs didn't exhibit obvious inhibition effects on cell proliferation with the concentrations up to 50 μg/mL (Fig. S5†).

The cellular uptake was evaluated in HeLa cells by confocal laser scanning microscopy (CLSM). HeLa cells were incubated with 10 μg/mL of SNBDP NCs for 0.5 h and 2 h. The cell nuclei were dyed with 4',6-diamidino-2-phenylindole (DAPI). The intensity of green fluorescence increased with prolonging incubation time from 0.5 h to 2 h (Fig. 5), indicating that SNBDP NCs could be internalized and located in the cytoplasm. It is worthy to mention that some green fluorescence could be seen in nuclei after 2 h incubation, showing that SNBDP NCs or BDP could escape from endosomes. It is well known that the endosomal escape is important and necessary for nanomedicine.[47] The reduction-responsive SNBDP NCs were assessed in the intracellular environment. HeLa cells were pretreated with 10 mM GSH according to the reported protocol,[48] and then incubated with SNBDP NCs for 0.5 h. The cells without pretreatment of GSH were used as controls. As expected, the stronger green fluorescence was observed in cells pretreated by GSH (Fig. S6†). As reported previously, GSH pretreatment did not significantly affect the endocytosis ability of cells.[49] So it could be inferred that the enhanced fluorescence intensity was ascribed to the rapid disassembly of SNBDP NCs.

In order to demonstrate the potential of SNBDP NCs as drugs carriers, rhodamine B (RhB) as a model drug was loaded into SNBDP NCs. The RhB-loaded NCs (RhB@SNBDP NCs) were prepared by adding THF solution of SNBDP into RhB solution. The average diameter of RhB@SNBDP NCs was 230.3 nm, which was slightly larger than that of SNBDP NCs because of introduced RhB (Fig. S7†). The fluorescence spectra of RhB@SNBDP NCs exhibited a red shift compared to RhB because of the aggregation of RhB in NCs (Fig. S8†). The

ARTICLE

cellular uptake was evaluated in HeLa cells by CLSM (Fig. 6). The red fluorescence of RhB was colocalized exactly with the green fluorescence of BDP, which confirmed that SNBDP NCs could encapsulate hydrophilic cargos and transport them (such as organic dyes and anti-cancer drugs) into the cells.

ICG-loaded SNBDP NCs

As mentioned above, SNBDP NCs could be potentially used as
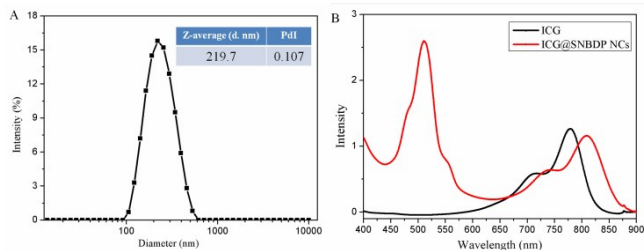
Fig. 7 (A) The size and PdI of the ICG@SNBDP NCs. (B) UV-vis absorption of ICG and the ICG@SNBDP NCs.

drug carriers to deliver therapeutic agents. Herein, ICG was chosen as a typical drug to study the drug delivery behaviours. ICG-loaded NCs (ICG@SNBDP NCs) were prepared as below. The THF solution of SNBDP was added into the aqueous solution of ICG, and the mixture was stirred, then dialyzed to remove THF and free small molecules. When an ICG content of 20 wt% was used in feed, the ICG-loaded NCs (ICG@SNBDP NCs) with loading efficiency of 46.3 % were obtained. The content and concentration of ICG was calculated to be 9.2 wt% and 11.1 μg/mL according to the standard curve, respectively.

The size and morphology of ICG@SNBDP NCs were studied by DLS (Fig. 7A) and TEM (Fig. S9†), respectively. The average diameter of ICG@SNBDP NCs was 219.7 nm and the PDI was 0.107. The size of ICG@SNBDP NCs was bigger than that of SNBDP NCs because of the loading of ICG. Enhanced contrast for ICG@SNBDP NCs as revealed by TEM (Fig. S9†) confirmed the successful encapsulation of ICG. The optical properties of the ICG@SNBDP NCs were recorded by UV-vis spectrometry. The maximum absorption of ICG@SNBDP NCs exhibited a red shift compared with free ICG because of the aggregation of ICG, which also confirmed that ICG was encapsulated into SNBDP NCs (Fig. 7B).

ICG has been demonstrated to be an effective photothermal agent.[50] The temperature of ICG@SNBDP NCs solution with ICG content of 11.1 μg/mL increased from 20.3 °C to 46.4 °C upon irradiation of 808 nm laser with 1 W/cm^2 for 3 min (Fig. 8A). Temperature reached to 36 °C when the concentration of ICG in NCs was 5.55 μg/mL. As a control, the SNBDP NCs solution showed little increase of temperature at the same condition. It was worth to mention that the temperature of free ICG solution only reached to 30.2 °C at the concentration of 11.1 μg/mL, which was much lower than that of ICG@SNBDP NCs. The enhanced photothermal effect was ascribed to the aggregate of ICG in NCs. These results indicated the great potential of nanoparticles-based photothermal agents. Many nanoparticles encapsulating ICG indicated the enhanced photothermal effect because of aggregation of ICG. The main reason for using stimuli-responsive NCs is based

on the requirement of cancer treatment in vivo. Moreover, controlled release and biodegradation are very important for drug delivery system. NCs could burst and degrade controllably by stimuli-responsive behavior because the NCs have to biodegrade after photothermal therapy.

Then the cellular uptake of was evaluated in HeLa cells by CLSM (Fig. S10†). The green fluorescence of BDP was clearly seen in the cytoplasm, which confirmed that the ICG-loaded NCs could be internalized into cells. Then we tested water-bath hyperthermia.[51] HeLa cells were exposed to 5 min of water-bath hyperthermia (45 °C and 50°C), which did not lead to significant increase in cancer cell death (Fig. S11†). At last, the photothermal therapy experiment towards HeLa cells was carried out. HeLa cells were incubated with different concentrations of ICG@SNBDP NCs for 5 h and then irradiated by the 808 nm laser for 5 min. The cells were incubated for another 18 h, then the cell viabilities were measured by CCK-8 method. More than 80 % of cells were killed after laser irradiation with the concentration of ICG at 10.3 μg/mL (Fig. 8B). In contrast, cells without ICG@SNBDP
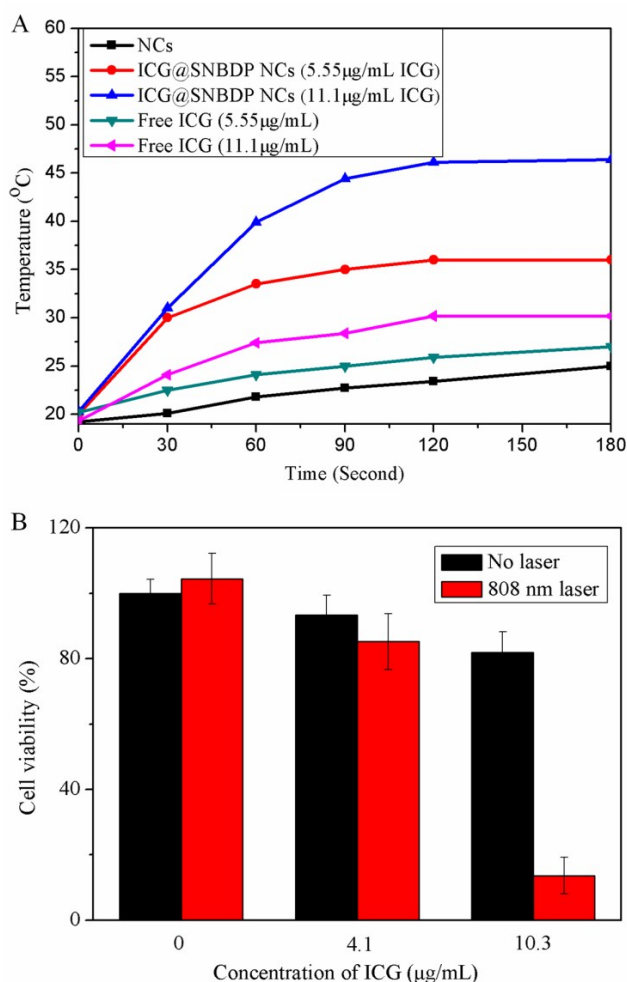
Fig. 8 (A) Heating curves of the ICG@SNBDP NCs and free ICG under NIR laser irradiation with different concentrations. (B) Relative cell viabilities of HeLa cells incubated with different concentrations of ICG@SNBDP NCs without or with laser irradiation (808 nm, 2.0 W/cm^2, 5 min). All the results were repeated three times and presented as mean ± SD.

NCs incubation or laser irradiation did not show obvious death. These results demonstrated that ICG@SNBDP NCs kept the effective photothermal activity for cancer therapy.

Conclusions

This work emphasizes that small molecules based nanocapsules are promoted by the insertion of a single disulfide bond into hydrophobic molecules, and the potential of using multi-component Passerini reaction to develop stimuli-sensitive materials. The DSINM technology, a new way of self-assembly, extends our knowledge of self-assembly and would stimulate the development of functional nanoparticles in various fields. Much work should be done to verify that the DSINM is a universal method for small molecules to self-assemble into nanoparticles. Secondly, multi-component reactions with isocyanides like Passerini reaction and Ugi reaction shows great potential to synthesize multi-functional molecules in mild conditions.

Acknowledgements

Notes and references

1   H. Zhang, J. Fei, X. Yan, A. Wang and J. Li, *Adv. Funct. Mater.*, 2015, **25**, 1193-1204.
2   S. H. Kim, J. A. Kaplan, Y. Sun, A. Shieh, H. L. Sun, C. M. Croce, M. W. Grinstaff and J. R. Parquette, *Chem. Eur. J.*, 2015, **21**, 101-105.
3   F. J. M. Hoeben, P. Jonkheijm, E. W. Meijer and A. P. H. J. Schenning, *Chem. Rev.*, 2005, **105**, 1491-1546.
4   J. Pecher and S. Mecking, *Chem. Rev.*, 2010, **110**, 6260-6279.
5   Y. Zhang, F. Ye, W. Sun, J. Yu, I. C. Wu, Y. Rong, Y. Zhang and D. T. Chiu, *Chem. Sci.*, 2015, **6**, 2102-2109.
6   I. C. Wu, J. Yu, F. Ye, Y. Rong, M. E. Gallina, B. S. Fujimoto, Y. Zhang, Y.-H. Chan, W. Sun, X.-H. Zhou, C. Wu and D. T. Chiu, *J. Am. Chem. Soc.*, 2015, **137**, 173-178.
7   Q. Zhao, X. Zhou, T. Cao, K. Y. Zhang, L. Yang, S. Liu, H. Liang, H. Yang, F. Li and W. Huang, *Chem. Sci.*, 2015, **6**, 1825-1831.
8   I. Fischer, K. Petkau-Milroy, Y. L. Dorland, A. P. Schenning and L. Brunsveld, *Chem. Eur. J.*, 2013, **19**, 16646-16650.
9   I. Fischer, A. Kaeser, M. A. Peters-Gumbs and A. P. Schenning, *Chem. Eur. J.*, 2013, **19**, 10928-10934.
10 F. Rodler, B. Schade, C. M. Jager, S. Backes, F. Hampel, C. Bottcher, T. Clark and A. Hirsch, *J. Am. Chem. Soc.*, 2015, **137**, 3308-3317.
11 P. Huang, D. Wang, Y. Su, W. Huang, Y. Zhou, D. Cui, X. Zhu and D. Yan, *J. Am. Chem. Soc.*, 2014, **136**, 11748-11756.
12 Z. Li, M. Zheng, X. Guan, Z. Xie, Y. Huang and X. Jing, *Nanoscale*, 2014, **6**, 5662-5665.
13 Y. Wang, D. Liu, Q. Zheng, Q. Zhao, H. Zhang, Y. Ma, J. K. Fallon, Q. Fu, M. T. Haynes, G. Lin, R. Zhang, D. Wang, X. Yang, L. Zhao, Z. He and F. Liu, *Nano Lett.*, 2014, **14**, 5577-5583.
14 X. Wu, B. Lin, M. Yu, L. Yang, J. Han and S. Han, *Chem. Sci.,* 2015, **6**, 2002-2009.
15 A. F.-j. Jou, C.-H. Lu, Y.-C. Ou, S.-S. Wang, S.-L. Hsu, I. Willner and J.-a. A. Ho, *Chem. Sci.*, 2015, **6**, 659-665.
16 X. Wu, S. Chang, X. Sun, Z. Guo, Y. Li, J. Tang, Y. Shen, J. Shi, H. Tian and W. Zhu, *Chem. Sci.*, 2013, **4**, 1221-1228.
17 M. J. Ruedas-Rama, J. D. Walters, A. Orte and E. A. H. Hall, *Anal. Chim. Acta*, 2012, **751**, 1-23.
18 T. Nakamura, F. Sugihara, H. Matsushita, Y. Yoshioka, S. Mizukami and K. Kikuchi, *Chem. Sci.*, 2015, **6**, 1986-1990.
19 M. Zheng, S. Liu, J. Li, D. Qu, H. Zhao, X. Guan, X. Hu, Z. Xie, X. Jing and Z. Sun, *Adv. Mater.*, 2014, **26**, 3554-3560.
20 L. Quan, S. Liu, T. Sun, X. Guan, W. Lin, Z. Xie, Y. Huang, Y. Wang and X. Jing, *ACS Appl. Mater. Interfaces*, 2014, **6**, 16166-16173.
21 M. Chen and M. Yin, *Prog. Polym. Sci.*, 2014, **39**, 365-395.
22 H. Xu, Q. Li, L. Wang, Y. He, J. Shi, B. Tang and C. Fan, *Chem. Soc. Rev.*, 2014, **43**, 2650-2661.
23 S. K. Yang, X. Shi, S. Park, T. Ha and S. C. Zimmerman, *Nat. Chem.*, 2013, **5**, 692-697.
24 A. Loudet and K. Burgess, *Chem. Rev.*, 2007, **107**, 4891-4932.
25 A. Vazquez-Romero, N. Kielland, M. J. Arevalo, S. Preciado, R. J. Mellanby, Y. Feng, R. Lavilla and M. Vendrell, *J Am. Chem. Soc.*, 2013, **135**, 16018-16021.
26 Y.-Z. Wang, X.-X. Deng, L. Li, Z.-L. Li, F.-S. Du and Z.-C. Li, *Polym. Chem.*, 2013, **4**, 444-448.
27 L. Li, A. Lv, X.-X. Deng, F.-S. Du and Z.-C. Li, *Chem. Commun.*, 2013, **49**, 8549-8551.
28 O. Kreye, T. Toth and M. A. Meier, *J. Am. Chem. Soc.*, 2011, **133**, 1790-1792.
29 A. Sehlinger, O. Kreye and M. A. R. Meier, *Macromolecules*, 2013, **46**, 6031-6037.
30 W. Lin, X. Guan, T. Sun, Y. Huang, X. Jing and Z. Xie, *Colloids Surf. B: Biointerfaces*, 2015, **126**, 217-223.
31 W. Lin, T. Sun, M. Zheng, Z. Xie, Y. Huang and X. Jing, *RSC Adv.*, 2014, **4**, 25114.
32 S. Choi, J. Bouffard and Y. Kim, *Chem. Sci.*, 2014, **5**, 751-755
33 H. Lu, Z. Xue, J. Mack, Z. Shen, X. You and N. Kobayashi, *Chem. Commun.*, 2010, **46**, 3565-3567.
34 C. Ren, H. Wang, D. Mao, X. Zhang, Q. Fengzhao, Y. Shi, D. Ding, D. Kong, L. Wang and Z. Yang, *Angew. Chem. Int. Ed.*, 2015, **54**, 4823-4827.
35 P. Hohenberg and W. Kohn, *Phys. Rev.*, 1964, **136**, B864-B871.
36 P. J. Stephens, F. J. Devlin, C. F. Chabalowski and M. J. Frisch, *J. Phys. Chem.*, 1994, **98**, 11623-11627.
37 A. D. Becke, *J. Chem. Phys.*, 1993, **98**, 5648-5652.
38 L. Yang, G. Fan, X. Ren, L. Zhao, J. Wang and Z. Chen, *Phys. Chem. Chem. Phys.*, 2015, **17**, 9167-9172.
39 U. Paiphansiri, G. Baier, A. Kreyes, D. Yiamsawas, K. Koynov, A. Musyanovych and K. Landfester, *Macromol. Chem. Phys.*, 2014, **215**, 2457-2462.
40 V. Ramamurthy and S. Gupta, *Chem. Soc. Rev.*, 2015, **44**, 119-135.
41 J. Zhao, J. Liu, S. Xu, J. Zhou, S. Han, L. Deng, J. Zhang, J. Liu, A. Meng and A. Dong, *ACS Appl. Mater. Interfaces*, 2013, **5**, 13216-13226.
42 Y. Gao, H. Qiu, H. Zhou, X. Li, R. Harniman, M. A. Winnik and I. Manners, *J. Am. Chem. Soc.*, 2015, **137**, 2203-2206.
43 S. Mura, J. Nicolas and P. Couvreur, *Nat. Mater.*, 2013, **12**, 991-1003.
44 G. Pasparakis, T. Manouras, M. Vamvakaki and P. Argitis, *Nat. Commun.*, 2014, **5**, 3623-3631.
45 T. Oda, T. Hayano, H. Miyaso, N. Takahashi and T. Yamashita, *Blood*, 2007, **109**, 5016-5026.

46 M. Yamagishi, K. Nakano, A. Miyake, T. Yamochi, Y. Kagami, A. Tsutsumi, Y. Matsuda, A. Sato-Otsubo, S. Muto, A. Utsunomiya, K. Yamaguchi, K. Uchimaru, S. Ogawa and T. Watanabe, *Cancer cell*, 2012, **21**, 121-135.

47 A. P. Blum, J. K. Kammeyer, A. M. Rush, C. E. Callmann, M. E. Hahn and N. C. Gianneschi, *J. Am. Chem. Soc.,* 2015, **137**, 2140-2154.

48 L. Yan, W. Wu, W. Zhao, R. Qi, D. Cui, Z. Xie, Y. Huang, T. Tong and X. Jing, *Polym. Chem.,* 2012, **3**, 2403.

49 H.-Y. Wen, H.-Q. Dong, W.-j. Xie, Y.-Y. Li, K. Wang, G. M. Pauletti and D.-L. Shi, *Chem. Commun.*, 2011, **47**, 3550-3552.

50 X. Sun, C. Wang, M. Gao, A. Hu and Z. Liu, *Adv. Funct. Mater.*, 2015, **25**, 2386-2394.

51 B. P. Shah, N. Pasquale, G. De, T. Tan, J. Ma and K.-B. Lee, *ACS Nano*, 2014, **8**, 9379-9387.

Chemical Science Accepted Manuscript